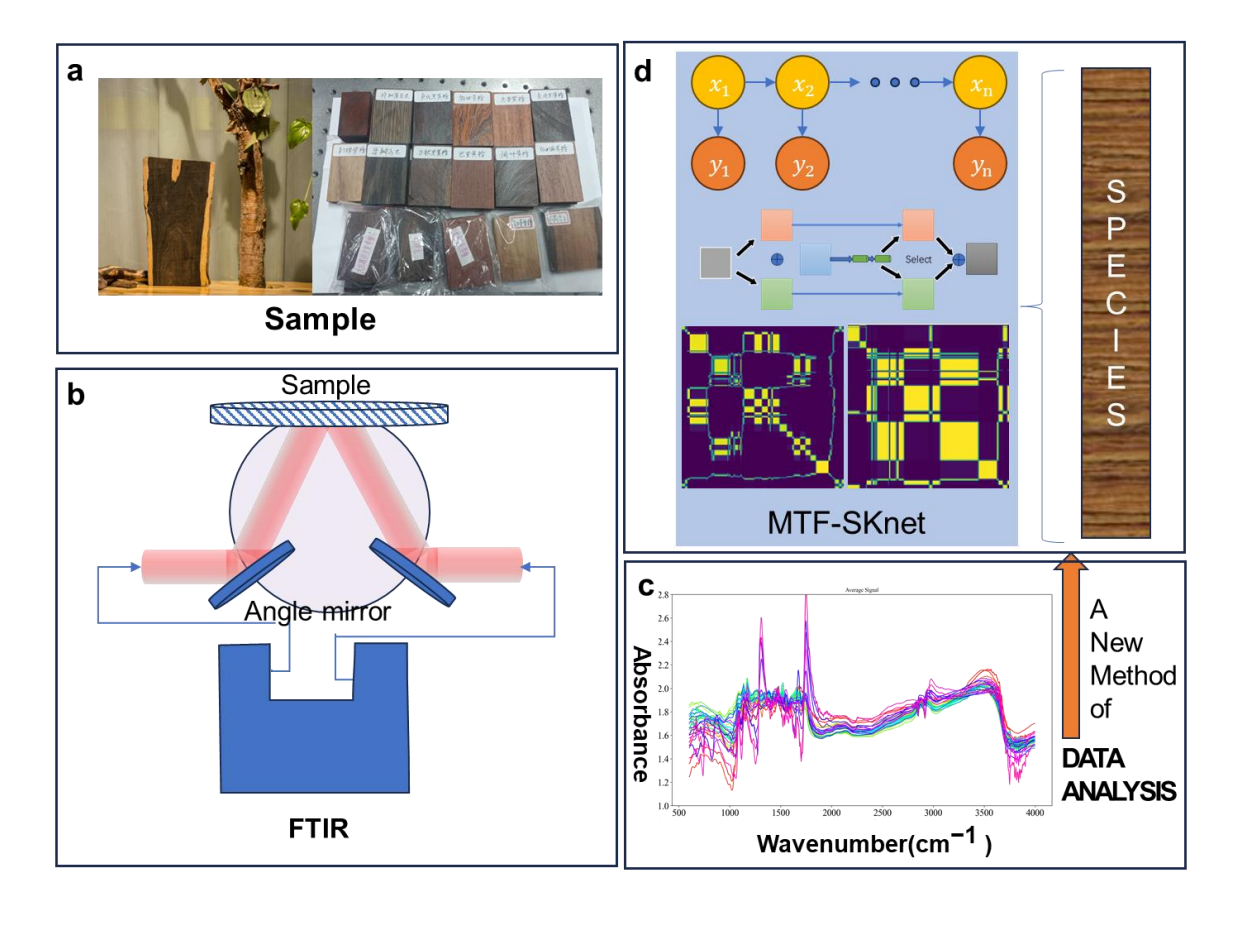
Application of MTF-SKNet for Wood Species Classification Using Mid-Infrared Spectroscopy

Ying-Jian Xin , a,c Pei-Pei Fang, a,b,c Hong-Peng Wang, a and Xiong Wan, a,*

* Corresponding author: wanxiong@mail.sitp.ac.cn

DOI: 10.15376/biores.20.2.4464-4478

GRAPHICAL ABSTRACT



Application of MTF-SKNet for Wood Species Classification Using Mid-Infrared Spectroscopy

Ying-Jian Xin , a.c Pei-Pei Fang, a,b,c Hong-Peng Wang, a and Xiong Wan, a,*

With the recovery of the economy and growth of living standards, the demand for wood furniture is increasing, leading to a focus on wood quality and market value. Mid-infrared (MIR) spectroscopy, which characterizes molecular vibrations, is well-suited for wood classification due to its ability to identify molecular structures. This study utilizes a Fourier Transform Infrared (FTIR) spectrometer to classify 31 wood species based on their commercial categories. While the basic composition of wood species is similar, spectral data are overall close, necessitating a robust approach for accurate identification. To address this, a two-dimensional transformation of the spectral data is performed, to convert wavenumber sequence and state transition probabilities (quantized intensity levels) of spectra into a matrix, followed by deep learning classification using the transformed data. This resulted in the development of the MTF-SKNet model, achieving a classification accuracy of 93% for wood species. The model demonstrated strong generalization performance, reaching 96% accuracy in classifying the rosewood category of woods.

DOI: 10.15376/biores.20.2.4464-4478

Keywords: Mid-infrared spectroscopy; Wood classification; Selective Kernel network; Markov transition field

Contact information: a: Key Laboratory of Space Active Opto-Electronics Technology of the Chinese Academy of Sciences, Shanghai Institute of Technical Physics, Chinese Academy of Sciences, Shanghai 200083, China; b: Key Laboratory of Systems Health Science of Zhejiang Province, School of Life Science, Hangzhou Institute for Advanced Study, University of Chinese Academy of Sciences, Hangzhou 310024, China; c: University of the Chinese Academy of Sciences, Beijing 100049, China;

* Corresponding author: wanxiong@mail.sitp.ac.cn

INTRODUCTION

Against the backdrop of China's rapid economic growth, the wood products industry is also developing swiftly, leading to a steady increase in the demand for timber. Currently, China's timber trade is characterized by supplementary import trade, with approximately 80% of the timber being imported (Ding and Yin 2024). The variety of imported wood species is vast, and the sources of timber are complex. The large market size makes it prone to trade frauds such as tariff evasion and the passing off of inferior goods as superior. In the new situation, accurately identifying wood species holds practical significance for stabilizing the market and protecting consumer interests.

Traditional methods of wood identification primarily include morphological observation and chemical composition analysis (Abe 2016). Morphological observation relies on the inspection of the wood's macro and microstructures, such as ring width, vessel morphology, and grain patterns. While this method is simple, it is often influenced by the observer's experience and technical level, with a high degree of subjectivity and difficulty in distinguishing wood species with similar appearances. Chemical composition analysis

involves qualitative and quantitative analysis of the wood's chemical components using chemical reagents, such as the determination of cellulose, hemicellulose, and lignin content. However, this method is complex, requires specialized equipment and reagents, and may cause damage during sample processing, making it time-consuming. Especially when dealing with a wide variety of tree species, manual identification can be very time-consuming and labor-intensive, necessitating an efficient and non-destructive identification method.

Significant progress has been made in the use of spectroscopy for wood analysis, with both mid-infrared (MIR, 400 to 4000 cm⁻¹) and near-infrared (NIR, 12500 to 4000 cm⁻¹) technologies demonstrating effectiveness and accuracy (Huang *et al.* 2008; Li *et al.* 2015; Shi *et al.* 2018; Pan *et al.* 2023; Das *et al.* 2024; Jesus *et al.* 2024).

Before classifying using spectral data, preprocessing is necessary to better summarize features for classification algorithms and achieve better classification results. Various other algorithms, such as Standard Normal Variate (SNV) and Multiplicative Scatter Correction (MSC), have been applied in the preprocessing process to obtain satisfactory preprocessing effects (Mou *et al.* 2013; Grisanti *et al.* 2018). Previous research has focused on developing classification models for wood species identification, using machine learning algorithms such as PCA-SVM, PLSDA, and SIMCA to directly classify the basic types of trees (Jesus *et al.* 2024). Although these existing methods have contributed to wood species identification, they often lack generalization ability, especially in distinguishing between high-value and low-value wood species, which is the research objective of this paper—to differentiate material value directly based on features.

To enhance generalization ability, deep learning comes to mind, as richer representational information and larger neural networks can better summarize the common characteristics of high and low value between different species. Studies using microscopic images have confirmed this (Ma, Kimura *et al.* 2024). Most current neural networks use two-dimensional data, requiring two-dimensional input for better training effects. This has led to the emergence of Two-Dimensional Correlation Spectroscopy (2DCOS), which transforms spectra into two-dimensional structures (Jiang and Rieppo 2006). Other two-dimensional methods, such as Gramian Angular Field (GADF) and Recurrence Plots (RP), can also be implemented (Pan *et al.* 2023; Das *et al.* 2024). However, these studies have not deeply investigated the intra-species differences, only highlighting the inter-species differences between different wood species. Addressing these limitations is crucial for developing more robust and comprehensive wood analysis techniques.

The purpose of this study is to construct an algorithm having high generalization capability, which combines intraspecific and interspecific spectral data characteristics, to achieve the identification of high-value rosewoods and non-rosewoods. The research utilized Fourier transform mid-infrared spectroscopy to collect data from 31 wood species, which were then processed with Multivariate Scattering Correction (MSC). Pearson correlation coefficient (Matsumoto *et al.* 2016) matrix calculations combined with hierarchical clustering analysis (Saxena *et al.* 2017) were performed on the processed data to identify the characteristic positions of intraspecific and interspecific differences. Subsequently, an attempt was made to convert the data into state probability maps using Markov Transition Fields (MTF) (Zhao *et al.* 2022), which served as input data for the optional Convolutional Neural Network (SKNet) model training (Li *et al.* 2019). The classification results were compared with other algorithms, verifying the effectiveness of the MTF-SKNet algorithm and demonstrating its universality and scalability in the qualitative analysis of wood mid-infrared spectra.

The innovations of this study are twofold. The first lies in the comparison of the intraspecific and interspecific difference characteristics of wood using Pearson correlation coefficient and hierarchical clustering analysis before developing the algorithm, whereas other papers only discussed the interspecific differences without comparing the midinfrared spectral characteristic differences within the same wood species. The second innovation is the development of an algorithm based on these characteristics, which can simultaneously handle the distinction between small tree species and the broader classification of rosewoods and non-rosewoods. Other papers aim at distinguishing small tree species and do not focus on the higher-level categorization of wood value, such as whether or not it belongs to the rosewood category.

EXPERIMENTAL

Samples

A total of 31 wood species were used in the study, including 19 national standard rosewood species and 12 non-rosewood species (Table 1). Each species had two samples with dimensions of approximately 60 mm x 40 mm x 10 mm, as shown in Fig. 1a. During testing, each wood sample was divided into four regions with a cross shape on both the front and back sides, and eight data points were collected from the center of each region, resulting in a total of 480 data points. The samples were provided by Yushan Town Xie-Qiao Huo-Men Rosewood Furniture Factory (Changshu City, Jiangsu Province, China) and they followed industry-standard protocols (air-dried, sanded to 400-grit).

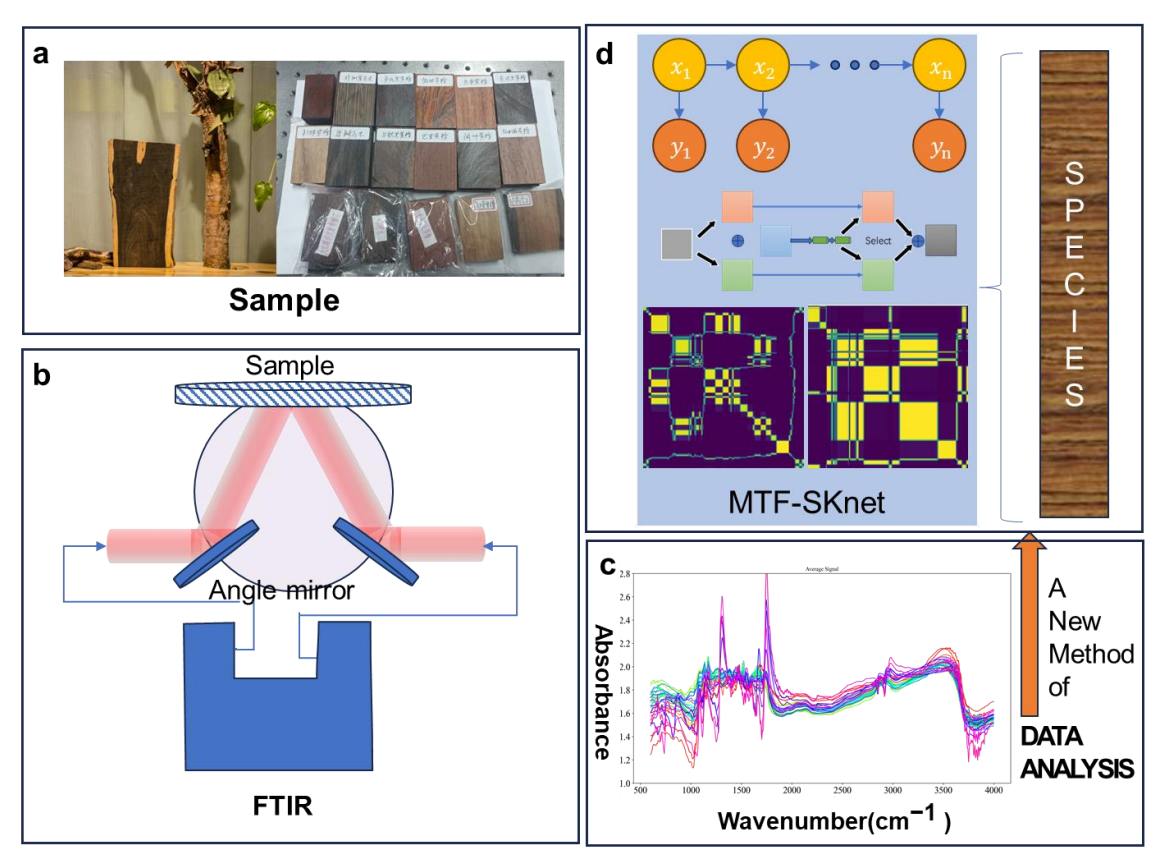


Fig. 1. Experimental process diagrams: (a) sample, (b) apparatus, (c) spectral data, (d) algorithm structure

Species/	Rosewood (Latin name)	Non-rosewood		
Category	Dalbergia melanoxylon	Black walnut wood		
	Dalbergia granadillo	North American black walnut wood		
	Diospyros ebenum	Polished North American black walnut wood		
	Dalbergia stevensonii	Polished northern walnut wood		
	Dalbergia cultrata	Northern walnut wood		
	Pterocarpus erinaceus	Southern walnut		
	Dalbergia louvelii	Polished southern walnut		
	Pterocarpus indicus	Wood bean (Pahudia javanica)		
	Diospyros crassiflora	European ash (Fraxinus excelsior)		
	Dalbergia cearensis	Polished European ash		
	Pterocarpus dalbergioides	Walnut-colored oak		
	Dalbergia bariensis	Faded walnut-colored oak		
	Diospyros pilosanthera			
	Diospyros celebica			
	Diospyros philippensis			
	Cassia siamea			
	Dalbergia latifolia			
	Millettia laurentii			
	Millettia leucantha			
Total number	19	12		

Table 1. Sample List (Species of Rosewood; GB/T 18107 2017)

Equipment

A Fourier transform infrared (FTIR) spectrometer (model MB3000, ABB, Zurich, Switzerland) was used for data acquisition. The instrument was equipped with a laboratory-built internal gold-coated integrating sphere for uniform illumination and scattered light collection, as well as a gold-coated reflector plate used as a reference material for calibrating the infrared light source. The system is shown in Fig. 1b.

All programs were run on a personal computer with the following specifications: GTX 1080 Ti graphics card, R5 5600X CPU, 32GB RAM.

Software

Horizon-MB (Zurich, Switzerland) was used to collect all the data from FTIR. The spectral data were collected within the range of 460 to 4000 cm⁻¹, with a resolution of 16 cm⁻¹, 64 scans, and an exposure time of 10 seconds. The data were output as absorbance values (Abs).

Python (Anaconda, Austin, TX, USA) was used to process the data, and draw some of pictures. This software was utilized for data preprocessing, feature extraction, model training, and evaluation. Libraries used include: NumPy: For numerical computing. SciPy: For scientific computing and signal processing. Pandas: For data manipulation and analysis. Scikit-learn: For machine learning algorithms and preprocessing. TensorFlow: For building and training deep learning models. PyTorch: For building and training deep learning models.

Origin-Pro (Origin-Lab Corporation, Northampton, MA, USA) was used for creating complex figures and visualizations.

Methods

Pre-process

In the preprocessing phase, signals were identified as irrelevant if they fell outside the operational spectral wavenumber range of the light source or were obscured by atmospheric absorption from water vapor and carbon dioxide. These irrelevant signals were removed to reduce interference and enhance data quality. Subsequently, noise reduction techniques were applied to eliminate the impact of noise on the signals. Finally, Multivariate Scattering Correction (MSC) was utilized to normalize the data, which helps to eliminate the effects of light scattering and baseline drift, ensuring consistency and comparability of the spectral data. This process made the spectral data more suitable for subsequent analysis and modeling. MSC is a preprocessing technique used in spectroscopy to correct for light scattering and baseline variations, enhancing the spectral quality for better analysis. It is commonly applied to improve the accuracy of chemical composition determination in samples by normalizing the spectra to account for instrumental and sample-related effects.

Analyze interspecific and intraspecific differences

The Pearson correlation coefficient and Hierarchical Clustering Algorithm (HCA) were used to find the biggest interspecific differences and the smallest intraspecific differences. The Pearson correlation coefficient measures the linear relationship between two signals, ranging from -1 (perfect negative correlation) to 1 (perfect positive correlation) (Matsumoto *et al.* 2016). It was calculated as follows,

$$r = \frac{\sum (x_i - \bar{x})(y_i - \bar{y})}{\sqrt{\sum (x_i - \bar{x})^2 (y_i - \bar{y})^2}} \tag{1}$$

where the Pearson correlation coefficient is represented by r, x_i , and y_i , which are paired observations of two variables, and \bar{x} and \bar{y} are the averages of these two variables.

The Hierarchical Clustering Algorithm is a commonly used clustering method that constructs a hierarchical tree of clusters by progressively merging or splitting existing clusters (Saxena *et al.* 2017). This method progressively merges existing clusters in a bottom-up approach. The agglomerative direction and the average linkage criterion were utilized as the method for determining the distance between clusters. The Pearson correlation coefficient was employed to measure the similarity between signals. Ultimately, this process results in a tree-like structure of the clusters.

MTF

The Markov Transition Field (MTF) method converts one-dimensional spectral data into a two-dimensional representation by encoding temporal dependencies through state transition probabilities (Zhao *et al.* 2022). This transformation involves three key steps:

- 1. State Quantization: The spectral intensity values are discretized into N distinct states (empirically optimized to N=10 in this study) based on intensity ranges.
- 2. Transition Probability Calculation: A Markov Transition Matrix (MTM) is constructed to capture the probability of transitioning between adjacent states along the spectral sequence. Each element $P_{i,j}$ in the MTM represents the likelihood of transitioning from state i to state j.
- 3. Image Generation: The MTM is mapped to a grayscale image matrix (Fig. 4a), where pixel intensity at position (i,j) corresponds to $P_{i,j}$. This matrix preserves dynamic

features (*e.g.*, peak shifts, intensity fluctuations) while suppressing noise through probabilistic smoothing. *SKNet*

The Selective Kernel Network (SKNet) enhances feature extraction in neural networks through a multi-scale architecture and adaptive attention mechanisms (Li *et al.* 2019). Its core design comprises three components (Fig.1.d):

- 1. Multi-Scale Convolution Branches: Parallel branches with varying kernel sizes (e.g., 3×3 and 5×5) extract local and global spectral features. For instance, smaller kernels capture fine-grained lignin aromatic vibrations (1600 to 1800 cm⁻¹), while larger kernels detect broad cellulose C-O stretching patterns (1000 to 1200 cm⁻¹).
- 2. Feature Fusion: A squeeze-and-excitation module aggregates multi-scale outputs, generating channel-wise attention weights to prioritize critical spectral regions (*e.g.*, lignin *vs.* cellulose-dominated bands).
- 3. Dynamic Kernel Selection: The attention weights dynamically adjust the contribution of each branch, enabling the model to adaptively focus on discriminative features (*e.g.*, subtle peak shifts in rosewood spectra).

SKNet, unlike standard CNNs with fixed kernel sizes, employs an adaptive selection mechanism that dynamically adjusts feature extraction across multiple kernel sizes. This attention-based approach contrasts with the static nature of traditional CNNs, offering a more efficient and focused feature representation with only a slight increase in parameters, making it particularly suitable for complex data analysis.

Result evaluation

The dataset was divided into a training set and a test set according to a 4:1 ratio. For each small category, if the number of individuals in the test set was greater than half of the category's individuals or equaled zero after intra-class division, a secondary replacement and redivision were performed. This means adjusting the number of test sets for that category and making up the difference with the test sets of other categories. This ensured the presence of test individuals without being too numerous.

After qualitative analysis of the dataset using the training set, the test set was used to evaluate the results. The accuracy rate of the actual test set results was compared to the algorithm's predicted results to assess the algorithm. Accuracy measures the performance of a classification model and represents the proportion of samples correctly predicted by the model out of all predicted samples, as follows,

$$Accuracy = \frac{TP + TN + FP + FN}{TP + TN} \tag{2}$$

where TP (True Positive) is the number of positive samples correctly predicted, TN (True Negative) is the number of negative samples correctly predicted, FP (False Positive) is the number of negative samples incorrectly predicted as positive, and FN (False Negative) is the number of positive samples incorrectly predicted as negative.

RESULTS AND DISCUSSION

Pre-processing

The light source signal was weak between the wavenumbers of 0 to 600 and 2300 to 2400, with strong signal fluctuation between 2300 to 2400, which is attributed to the mid-infrared absorption of carbon dioxide and water vapor gases. Typically, the method of

purging with nitrogen is used to remove these effects. However, in the course of this study, nitrogen purging was not employed. Consequently, during preprocessing, a truncation from 460 to 600 wavenumbers and a smoothing from 2300 to 2450 wavenumbers were added to reduce signal characteristics caused by non-sample factors.

The data results after preprocessing for one sample are shown in Fig. 2. For most samples, after preprocessing, the signal range area became smaller, indicating smaller intraspecific differences, which is beneficial for clustering based on intraspecific characteristics.

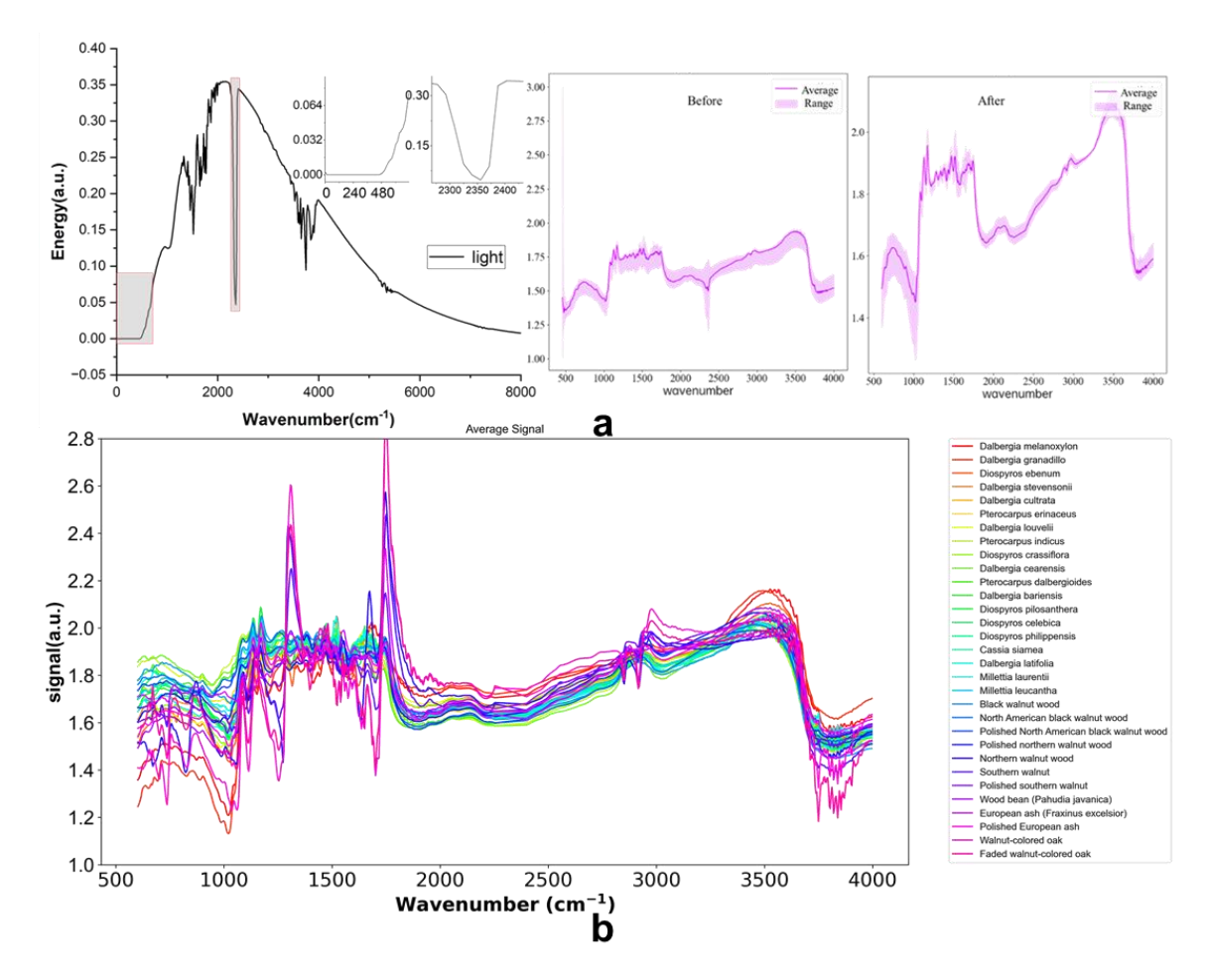


Fig. 2. Spectrum data. a. Reference light source comparison chart before and after preprocessing (using *Pterocarpus erinaceus* as an example) b. Average pre-processed spectrum for each wood species

Analyze interspecific and intraspecific differences

The Pearson correlation coefficients were calculated to obtain the intraspecific and interspecific correlation coefficient matrices. Using these matrices, hierarchical clustering with the average distance method was performed. The resulting dendrograms for intraspecific and interspecific clustering revealed that the two wood species with the largest intraspecific distances were *Dalbergia latifolia* and *Dalbergia louvelii*. The group with the smallest interspecific distance included *Pterocarpus indicus*, *Pterocarpus andamanicus*, *Dalbergia cearensis*, *Juglans nigra*, and *Juglans nigra* from North America, as well as *Diospyros ebenum*, *Diospyros crassiflora*, *Dalbergia louvelii*, *Machilus thunbergii*, *Pahudia javanica*, and *Fraxinus mandshurica*.

As shown in Fig. 3-a,b after preprocessing, the two species still exhibited significant intraspecific differences, primarily concentrated in two wave number ranges. The first range is between 600 to 1100 cm⁻¹, where generally, vibrations reflecting cellulose C-H deformation occur, with an appearance near 900 cm⁻¹. The absorption peak near 1050 cm⁻¹ corresponds to the C-O stretching vibration in cellulose and hemicellulose. The fluctuations in the fingerprint region below 900 cm⁻¹ are often influenced by C-H bonds in special structures, such as the aromatic ring C-H stretching near 850 cm⁻¹. The second range is between 1850 and 2800 cm⁻¹, where the spectrum is relatively smooth with fewer absorption peaks. There is a fixed envelope near 2100 cm⁻¹, which, as it is not mentioned in other wood-related studies, is speculated to be due to C=O (carbonyl) from the benzene ring of specific lignin monomers (such as p-coumaric acid) or the carbonyl on the pyran ring in cellulose carbonyl. This deviates from the original position.

As shown in Fig. 3-c,d, the interspecific differences between different species were relatively small after preprocessing, mainly concentrated in two wave number ranges. The first range is between 1100 and 1600 cm⁻¹, where there are more complex molecular bond vibrations, including C=O, aromatic, and C-O stretching vibrations, as well as alkyl vibrations on different carbon chains. The 1100 to 1600 cm⁻¹ range mainly involves lignin aromatic ring skeleton stretching vibrations and C=O, C-O-C, methyl C-H stretching deformation vibrations in lignin and cellulose. The peak segment between 1032 and 1037 cm⁻¹ is primarily due to lignin aromatic C-H in-plane deformation, in-plane bending, C-O deformation in primary alcohols, and non-conjugated C=O stretching. The 1245 cm⁻¹ corresponds to lignin syringyl ring vibration, and 1266 cm⁻¹ is the guaiacyl ring plus C-O stretching vibration. The 1630 to 1660 cm⁻¹ range corresponds to the vibration of amino compounds in protein peptides. The second range is at 3000 cm⁻¹.

 Table 2. Wood IR Vibrational Spectrum and Wavenumber Reference Table

No.	Wavenumber (cm ⁻¹)	Vibration			
1	835	Cellulose β-chain, stretching of C-H bonds extending out of			
		the aromatic ring plane			
2	898	Cellulose P-chain, stretching of C-H bonds extending out of			
		the aromatic ring plane			
3	1030	C-O vibration in secondary alcohols and fatty ethers			
4	1160	C-O-C stretching in the pyran ring, C=O stretching in			
		aliphatic groups			
5	1230	C-O-C stretching of phenol ether bonds in lignin			
6	1260	Guaiacol ring C–N–H stretching vibration in lignin			
7	1270	Stretching of guaiacyl unit G ring and O-C-O			
8	1317	Connecting bond between guaiacyl unit and coniferyl unit,			
		bending and stretching of coniferyl unit and CH2			
9	1375	O-H in methyl and phenol, and aliphatic C-H stretching			
		vibration			
10	1425	Stretching vibration of C-H in-plane bound to the aromatic			
		skeleton			
11	1463	Stretching vibration of CH2 in lignin and xylan			
12	1510	Aromatic skeleton stretching			
13	1619 / 1640	C=O stretching vibration in coumarin			
14	1740	C=O stretching vibration in unconjugated ketones,			
		carbonyls, and aliphatic groups (xylan)			
15	2930	C-H stretching vibration in methyl and methylene groups			
16	3400	O-H stretching vibration in hydroxyl groups			

By synthesizing the display of both interspecific and intraspecific differences above, one can observe that these differences mostly do not overlap. Therefore, it is not difficult to distinguish different types of wood using spectroscopy. As long as the model training process focuses on the characteristic information of the corresponding wavebands and uses it as a basis, the accuracy of the classification results can be ensured. This also provides a basis for the subsequent use of the SKNet network with a self-attention mechanism. All observed signal peaks wavenumber and their corresponding positions are recorded in Table 1 (Huang *et al.* 2008; Li *et al.* 2015; Shi *et al.* 2018; Liu *et al.* 2024).

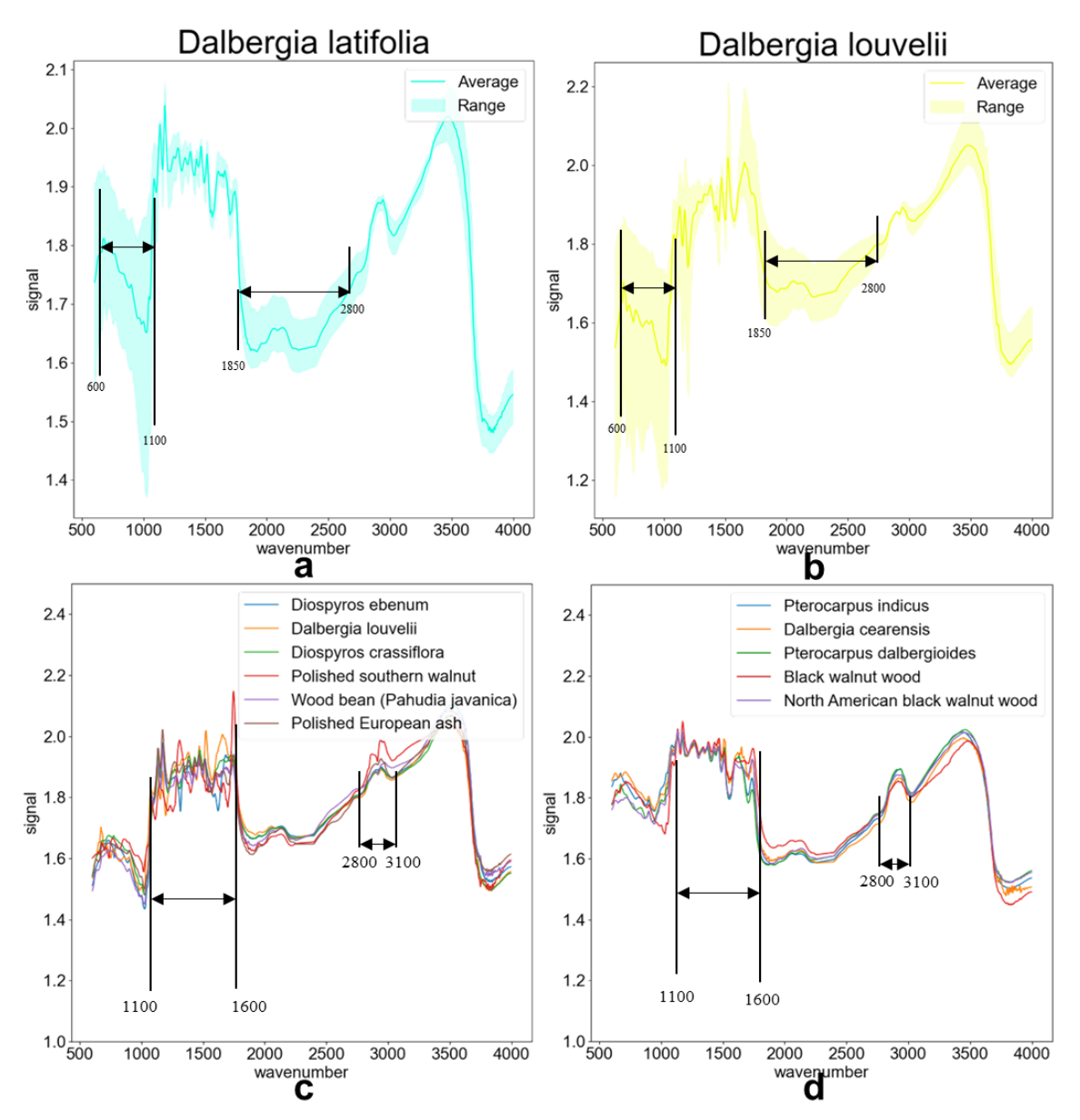


Fig. 3. FT-IR Interspecific and Intraspecific signal difference comparison chart

MTF

Four common methods for transforming one-dimensional mid-infrared data into two dimensions were compared: Gramian Angular Field (GAF), Markov Transition Field (MTF), Recurrence Plot (RP), and Two-Dimensional Correlation Spectroscopy (2DCOS).

The two-dimensional images obtained through these four methods are shown in Fig. 4. The Recurrence Plot retained the best details, but it lacked image blocks of varying sizes, which is not conducive to feature extraction. The Gramian Angular Field had a low redundancy of information, with detailed differences distributed at the edges of the image, which is beneficial for information retention. However, the details were concentrated, which can lead to blurred features. 2DCOS, typically used for analyzing coherent peaks between different signals, resulted in feature overlapping due to the calculation of the autocorrelation matrix. The Markov Transition Field selectively retains or discards local information based on state definitions, allowing for the focus on feature information relevant to the algorithm's objectives as the screening criterion. As Shown in Fig. 4e, for the 1850 to 2800 cm⁻¹ region, which is not of interest in classification, most images exhibited convergence, corresponding to no features being extracted. However, at the more significant glycosidic bond response position (1160 cm⁻¹) and the position of the aromaticrelated C-H bonds (1850 cm⁻¹), more signals were extracted, and the features were more pronounced. More states result in richer information about the details obtained, but they are more susceptible to noise. Therefore, it is necessary to determine the specific number of states for the MTF algorithm.

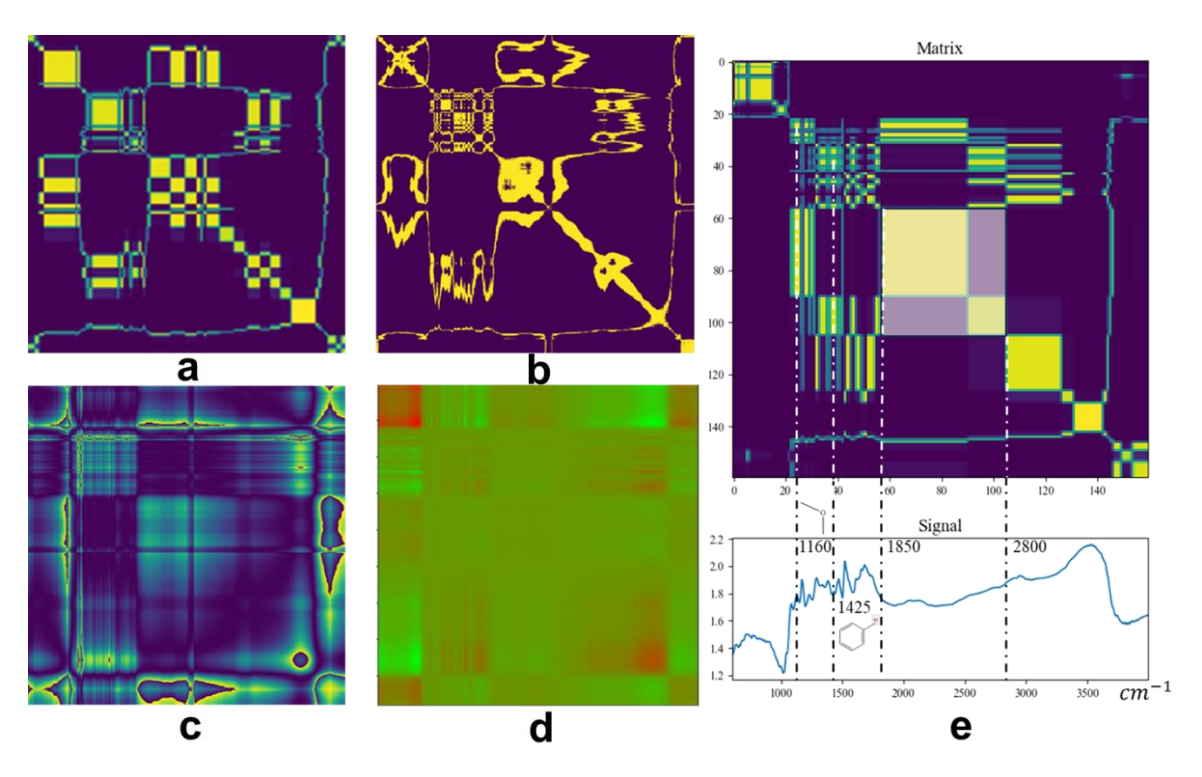


Fig. 4. Spectral data after the two-dimensional transformation:(a) Markov Transition Field (b) Recurrence Plot (c) Gramian Angular Field (d) Two-Dimensional Autocorrelation Spectroscopy (e) Spectral and matrix correlation diagram

For the MTF algorithm, it is necessary to determine the algorithm parameters, with the most critical parameter being the number of states. The greater the number of states, the stronger the information extraction capability of the Markov Transition Field, and the more details are preserved. However, the corresponding two-dimensional image becomes more complex, leading to poorer clustering results. The aim is to retain the features representing inter-species differences while filtering out the intra-species difference

features. By comparing the image transformation results with state numbers of 5, 10, 25, 50, and 100, as shown in Fig. 5, it was determined that a state number of 10 best met the computational expectations.

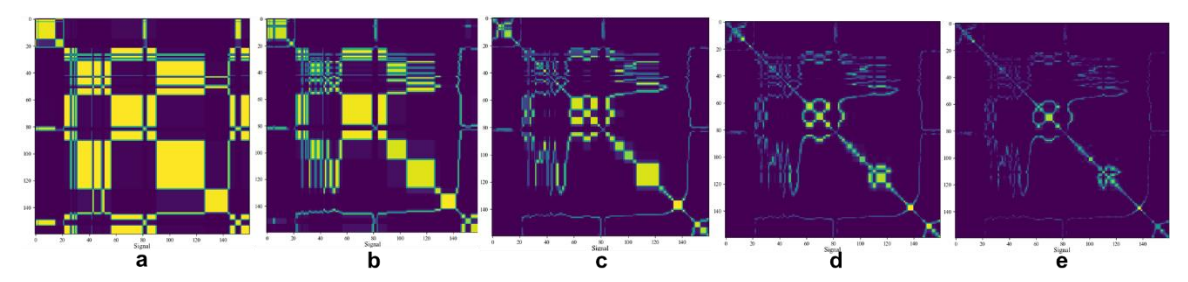


Fig. 5. Images of Markov transformation fields with different numbers of states

Evaluation

The comparative qualitative analysis methods include the following:

Method One: Directly input the preprocessed data into the Support Vector Machine (SVC). Support Vector Machine is a classification method based on the maximum margin principle, which is simple and efficient, suitable for medium and small-scale classification problems. By introducing a kernel function, SVC can effectively solve nonlinear classification problems and is applicable to this classification problem.

Method Two: Use Principal Component Analysis (PCA) to reduce the dimensionality of the preprocessed data and then classify using SVC (PCA-SVC). By reducing the dimensionality with PCA, the data dimensionality is reduced, the computational complexity is lowered, noise and redundant information are removed, which helps to improve the classification accuracy of SVC.

Method Three: Generate two-dimensional data using the Markov Transition Field and then classify using a Convolutional Neural Network (MTF-CNN). MTF can generate two-dimensional data with local correlations, which is beneficial for CNN to extract local features. CNN has superior performance in the field of image recognition and is suitable for complex classification problems.

Method Four: Generate two-dimensional data using the Markov Transition Field and then classify using the Selective Kernel Network (MTF-SKNet). SKNet can dynamically select the appropriate convolution kernels based on the features of the input data, improving classification performance. By processing data with different features in parallel with convolution kernels, it has strong adaptability. Most importantly, it maintains a high classification accuracy while reducing computational complexity, which is conducive to the application of practical problems.

Method Five: Generate two-dimensional data using the Random Projection (RP) method, and then classify using CNN (RP-CNN). RP transforms data into a lower-dimensional space, preserving the structure for CNN to process.

Method Six: Generate two-dimensional data using the Gramian Angular Field (GAF) and then classify using CNN (GAF-CNN). GAF captures temporal relationships, converting them into a format that CNN can effectively analyze for classification.

Method	SVC	PCA-SVC	MTF-CNN	MTF-SKNet	GAF-CNN	RP-CNN
Train Accuracy	61.2%	92.4%	91.6%	93.5%	71.4%	80.3%
Test Accuracy	55.6%	92.6%	86.2%	93.2%	70.1%	76.3%

Table 3. Comparison of Classification Accuracy Results for Wood Species

Comparing MTF-CNN, GAF-CNN, and RP-CNN, a clear difference becomes evident. MTF is key for feature extraction and noise reduction. It boosted classification accuracy by about 10% compared to GAF and RP. MTF-CNN vs. MTF-SKNet showed another layer of difference. SKNet excels in selecting and extracting feature scales. This is vital for complex 2D images. It improved accuracy by around 2 to 5%. The MTF-SKNet algorithm exhibited a marginally higher accuracy in comparisons, with PCA-SVC also achieving a commendable accuracy rate of 92.6%. The slight difference in accuracy between MTF-SKNet and PCA-SVC, with MTF-SKNet scoring 93.2%, underscores the importance of sophisticated feature extraction techniques in high-dimensional mid-infrared spectral data. SVC's lower accuracy can be attributed to the lack of effective feature extraction in high-dimensional mid-infrared spectral data, leading to poor classification. This highlights the significance of feature extraction and dimension reduction. SKNet's adaptability in extracting features of different sizes was demonstrated by its performance compared to MTF-CNN, ensuring accurate predictions. The experiment confirmed SKNet's suitability for MTF-generated two-dimensional data, with the confusion matrix for the predicted results shown in Fig. 6.

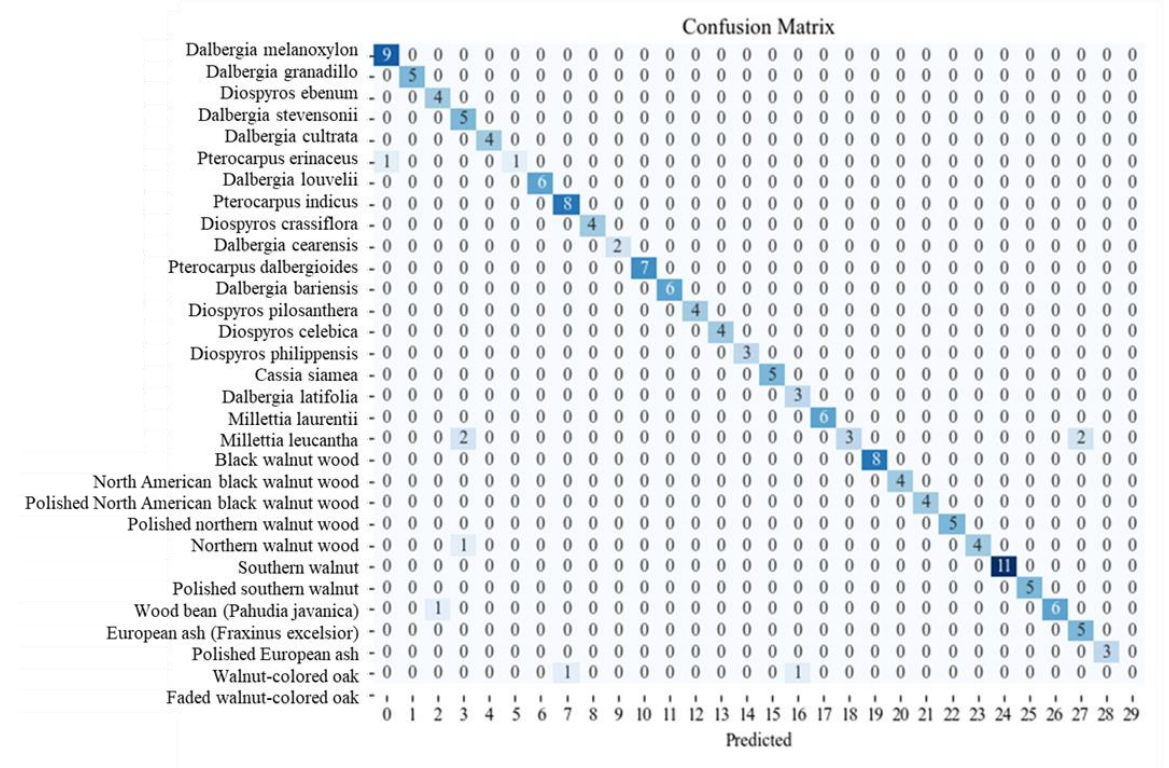


Fig. 6. Confusion Matrix of the MTF-SKNet Algorithm

The label is simplified to "Rosewood" and "non-Rosewood," thus turning the prediction results into a binary classification for the model. After retraining the model, an

independent dataset was employed that had been collected from separately purchased samples, which underwent the same processing methods as the previous samples. The dataset consisted of six species: three types of rosewood (*Dalbergia cochinchinensis*, *Dalbergia sissoo*, and *Dalbergia melanoxylon*) and three types of non-rosewood (*Pinus sylvestris*, *Populus adenopoda*, and *Quercus alba*), with five samples of each species, totaling 30 samples. This dataset was not involved in the model training process, ensuring the independence of the validation data. The accuracy rates of the algorithms are compared as follows:

Table 4. Comparison of Classification Accuracy Rates for Wood Category

Method	SVC	PCA-SVC	MTF-CNN	MTF-SKNet	RP-CNN	GAF-CNN
Accuracy	42.6%	85.6%	83.2%	96.0%	90.4%	79.7%

For directly representing binary classification, the MTF-SKNet algorithm reduces data details, extracts data features, and improves accuracy. Therefore, it has a higher resistance to label ambiguity compared to the PCA-SVC algorithm. This data reflects the stronger generalization ability of the MTF-SKNet algorithm.

CONCLUSIONS

- 1. The MTF-SKNet algorithm demonstrated robust performance in differentiating wood species and broader commercial categories, achieving 93.2% accuracy with strong generalization (96.0% for rosewood classification with new samples).
- 2. The hierarchical clustering analysis revealed that the spectral differences between species and within species are localized in distinct mid-infrared spectral regions, indicative of unique material composition variations among the tree samples studied.
- 3. The manual definition of state positions in the MTF two-dimensional method allows for the leveraging of prior knowledge, which is instrumental in the selective filtering and extraction of discriminative features from the spectral data.
- 4. The research underscores the potential of advanced machine learning techniques, such as the MTF-SKNet algorithm, for the accurate and efficient identification of wood species, which could have significant implications for the timber industry, conservation efforts, and regulatory compliance.
- 5. The findings of this study contribute to the broader understanding of the spectral characteristics of wood and the development of analytical methods that can be applied to a wide range of forensic, ecological, and industrial challenges.

ACKNOWLEDGMENTS

The authors are grateful for the support of the National Key R&D Program of China Grant No. 2021YFF0601201, 2021YFF0601202, 2021YFF0601200 and the National Natural Science Foundation of China Grant No. 42074210.

REFERENCES CITED

- Abe, H. (2016). "Importance and techniques of wood species identification," *Mokuzai Gakkaishi Journal* 62(6), 240-249. DOI: 10.2488/jwrs.62.240
- Das, S., Paramane, A., Chatterjee, S., and Mishra, P. (2024). "Recurrence plot-aided deep learning framework for condition monitoring of transformer insulation using Fourier transform infrared spectroscopy," *IEEE Transactions on Industry Applications* PP: 1-10. DOI: 10.1109/TIA.2024.3430254
- Ding, Y., and Yin, Z. (2024). "The study on the effect of restrictive rosewood trade policies on China's rosewood import prices," *Forestry Economics Review* 6. DOI: 10.1108/FER-11-2023-0011
- Grisanti, E., Totska, M., Huber, S., Calderon, C., Hohmann, M., Lingenfelser, D., and Otto M. (2018). "Dynamic localized SNV, peak SNV, and partial Peak SNV: Novel standardization methods for preprocessing of spectroscopic data used in predictive modeling," *Journal of Spectroscopy* 2018, 1-14. DOI: 10.1155/2018/5037572
- Huang, A., Zhou, Q., Liu, J., Fei, B., and Sun S. (2008). "Distinction of three wood species by Fourier transform infrared spectroscopy and two-dimensional correlation IR spectroscopy," *Journal of Molecular Structure* 883-884, 160-166. DOI: 10.1016/j.molstruc.2007.11.061
- Jesus, E., Franca, T., Calvani, C., Lacerda, M., Gonçalves, D., Oliveira, S., Marangoni, B., and Cena, C. (2024). "Making wood inspection easier: FTIR spectroscopy and machine learning for Brazilian native commercial wood species identification," *RSC Advances* 14, 7283-7289. DOI: 10.1039/d4ra00174e
- Jiang, E. Y., and Rieppo, J. (2006). "Enhancing FTIR imaging capabilities with two-dimensional correlation spectroscopy (2DCOS): A study of concentration gradients of collagen and proteoglycans in human patellar cartilage," *Journal of Molecular Structure* 799(1), 196-203. DOI: 10.1016/j.molstruc.2006.03.069
- Li, M.-Y., Cheng S.-C., Li D., Wang S.-N., Huang A.-M., and Sun, S.-Q. (2015). "Structural characterization of steam-heat treated Tectona grandis wood analyzed by FT-IR and 2D-IR correlation spectroscopy," *Chinese Chemical Letters* 26(2), 221-225. DOI: 10.1016/j.cclet.2014.11.024
- Li, X., Wang, W. H., Hu, X. L., Yang, J., and Soc, I. C. (2019). "Selective kernel networks," 32nd IEEE/CVF Conference on Computer Vision and Pattern Recognition (CVPR), Long Beach, CA, IEEE Computer Soc. DOI: 10.1109/cvpr.2019.00060.
- Ma, T., Kimura, F., Tsuchikawa, S., Kojima, M., and Inagaki, T. (2024). "Validation study on the practical accuracy of wood species identification *via* deep learning from visible microscopic images," *BioResources* 19(3), 4838-4851. DOI: 10.15376/biores.19.3.4838-4851.
- Matsumoto, T., Fuchita, Y., Ichikawa, K., Fukuda, Y., Takemura, N., and Sakatani, K. (2016). "Gender and age analyses of NIRS/STAI Pearson correlation coefficients at resting state," *Adv Exp Med Biol.* 876, 281-287. DOI: 10.1007/978-1-4939-3023-4 35.
- Mou, Y., You, X., Xu, D., Yu, S., Zhou, L., and Zeng, W. (2013). "Regularized multivariate scatter correction," *Chemometrics and Intelligent Laboratory Systems* 132. DOI: 10.1016/j.chemolab.2013.12.004
- Pan, X., Yu, Z. M., and Yang, Z. (2023). "A deep learning multimodal fusion framework for wood species identification using near-infrared spectroscopy GADF and RGB image," *Holzforschung* 77(11-12), 816-827. DOI: 10.1515/hf-2023-0062

- Saxena, A., Prasad, M., Gupta, A., Bharill, N., Patel, O. P., Tiwari, A., Er, M. J., Ding, W., and Lin, C.-T. (2017). "A review of clustering techniques and developments," *Neurocomputing* 267, 664-681. DOI: 10.1016/j.neucom.2017.06.053
- Shi, J., Lu, Y., Zhang, Y., Cai, L., and Shi, S. Q. (2018). "Effect of thermal treatment with water, H₂SO₄ and NaOH aqueous solution on color, cell wall and chemical structure of poplar wood," *Scientific Reports* 8(1), article 17735. DOI: 10.1038/s41598-018-36086-9
- Zhao, X. T., Sun, H. B., Lin, B., Zhao, H. M., Niu, Y. L., Zhong, X., Wang, Y. D., Zhao, Y. M., Meng, F. C., Ding, J. M., Zhang, X. H., Dong, L., and Liang, S. (2022). "Markov transition fields and deep learning-based event-classification and vibration-frequency measurement for φ-OTDR," *IEEE Sensors Journal* 22(4), 3348-3357. DOI: 10.1109/jsen.2021.3137006

Article submitted: January 27, 2025; Peer review completed: February 22, 2025; Revised version received and accepted: March 4, 2025; Published: April 28, 2025. DOI: 10.15376/biores.20.2.4464-4478